Original Research Article

J. Funct. Mater. Biomol. 2(1)-2018 pp 1-9

SACRED HEART RESEARCH PUBLICATIONS

Journal of Functional Materials and Biomolecules

Journal homepage: www.shcpub.edu.in

ISSN: 2456-9429

Investigation of Spinel $Ni_{0.5}Dy_{0.5}Fe_2O_4$ Nanoparticles by Facile Co-Precipitation Route and their Influence on the degradation of organic compound

P. Annie Vinosha[1], S. Deepapriya[1], John.D.Rodney[1], S. Krishnan[2] and S. Jerome Das[1*]

Received on 11 Apr 2018, Accepted on 12 May 2018

Abstract

Ferrite nanocrystals has sworn significant consideration in the current epoch owed to its unique environmental application in the degradation of organic pollutants and similarly its viability in technical and scientific zones of its significant properties such as, magnetical, electrical and optical. Nanosized ferrites are the utmost class of nanomaterials that have been significantly tailored by the research commune owing to their excellent properties. The properties present in $Ni_{0.5}Dy_{0.5}Fe_2O_4$ nanocrystal make it a fitting candidate in the field of applied electronics. A conceivable and thriftily viable chemical precipitation technique has been used in the synthesis of $Ni_{0.5}Dy_{0.5}Fe_2O_4$ nanocrystal. The as-synthesized nanopowders were analyzed to determine its properties like structural, optical, magnetical and photocatalytic activity. The structural property is depicted by powder X-ray diffraction (XRD), the formation of spinel peak was confirmed the crystallite size was calculated and found to increase as the pH concentration increased. TEM micrograph reveals the cubic nature and the crystallinity of the as-synthesized samples. The FTIR analysis elucidates the functional groups and the types of interionic bond present in the nanosamples, the two adsorption peaks were observed around 400 and 500 cm^{-1}. UV-visible analysis (UV-vis) elucidates the optical property of the as-synthesized and hence as the result photocatalytic activity was observed. By using vibrating sample magnetometer at room temperature, the magnetic properties were determined and various parameters were calculated.

Keywords: Co-precipitation; XRD, photo-Fenton.

1 Introduction

The occurrence of numerous macrobiotic contaminants in surface water and ground water may upshot from the polluted agricultural runoff, soil, industrial wastewater and perilous compounds storage seepage. The presence of these crude compounds in water poses grim peril to communal wellbeing while most of them are endocrine disrupting, toxic, carcinogenic or mutagenic to aquatic life, animals and humans in general. Numerous unrefined pollutants are considered as detrimental and toxic even, at very less concentration. For this rationale, their exclusion from the tainted water is of high priority. Accordingly, the necessity for proficient treatment of these contaminants is imperative. In certain cases, predictable treatment methods such as organic process are not effective due to the recalcitrant environment of the contaminants present [1, 2]. Therefore, the oxidation process is preferred to degrade such organics present. The water treatment process advanced oxidation processes, which involve the generation of hydroxyl radicals in sufficient quantity to affect water purification. The nano catalyst has been used in the degradation of the harmful organic compounds [3]. As an impending member of ferrite family, $Ni_{0.5}Dy_{0.5}Fe_2O_4$ nanocrystal has engrossed research community by its stimulating ferromagnetic nature. Inverse spinel ferrite nanoparticles possess a significant technological applications such as, a catalyst, recording devices, sensors, MRI, etc,. Nickel ferrite as an inverse spinel phase formation with the Fe^{3+}cations in the octahedral site which plays a significant role in the physical properties such as magnetic saturation, coercivity and high Curie temperature [4, 5]. The structural and magnetic properties depend on the ionic distribution as per the interaction of ions in the octahedral and tetrahedral sites these properties are tailored by the researchers by several synthesis techniques such as, co-precipitation [6], solvothermal [7], hydrothermal [8], microemulsion [9], combustion [10], etc,. Besides these methods, the co-precipitation technique is a probable one for tailoring the uniform distribution of nanoparticles at an optimum temperature. In the present study, an effort has been put to prepare the $Ni_{0.5}Dy_{0.5}Fe_2O_4$nanocrystal by the co-precipitation route. The synthesized nanomaterials were characterized by various techniques to investigate its properties. In the present study, Methylene blue (MB) dye was used as a mock-up pollutant and the degradation mechanism was studied in detailed with its recyclability, which makes itself a potential candidate in the industrial application.

* Corresponding author e-mail: jeromedas.s@gmail.com, jerome@loyolacollege.edu, Phone: +91-9094139314

[1] Department of Physics, Loyola College, Chennai, 600 034, India

[2] Department of Physics, Ramakrishna Mission Vivekananda College, Chennai- 600 004, India.

2 Experimental

Nickel nitrate hexahydrate $(Zn(NO_3)_2.6H_2O)$, Dysprosium nitrate hexahydrate $(Fe(NO_3)_2.6H_2O)$, ferric nitrate hexahydrate $(Fe(NO_3)_2.6H_2O)$ and sodium hydroxide pellets were acquired from Merck and utilized without further refinement. Nickel nitrate hexahydrate, Dysprosium nitrate hexahydrate and ferric nitrate hexahydrate are taken independently in 50 ml of distilled water and blended well till homogenization was achieved. The 2 M of sodium hydroxide (NaOH) was used as a mineralizer, in drop-wise into the admix solution under persistent blending in order to maintain the pH 9. The temperature was raised from 40 °C to 80 °C and kept for 2 h under constant stirring till the precipitate was obtained and then the precipitate was cooled to room temperature. In order to remove the nitrate ions and impurities the obtained by product was centrifuged twice with ethanol and distilled water at 7000 rpm. The obtained by-product was annealed at 75 °C for 12 h and then grounded for further calcination at 500 °C for 3 h, the obtained nano product was analyzed to determine its significant properties. Same procedure was followed for pH 10, 11 and 12.

3 Results and Discussion

3.1 XRD analysis

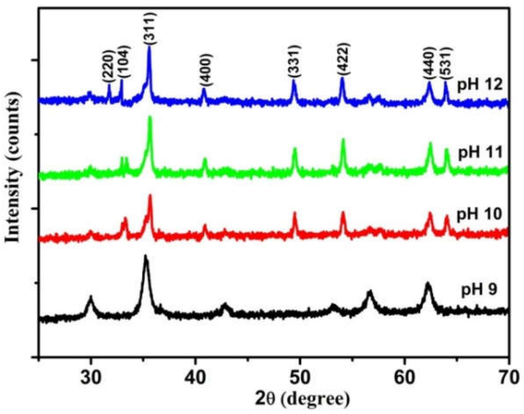

Fig.1a XRD pattern for $NiDyFe_2O_4$ nanocrystal

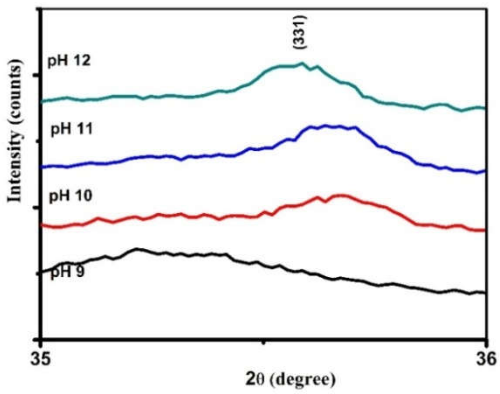

Fig.1b Deviation of (311) diffraction peak with respect to pH concentration

XRD pattern in **Fig. 1a** depicts the peaks engrossed to a typical spinel phase of $Ni_{0.5}Dy_{0.5}Fe_2O_4$nanocrystal, it is clear that the pattern had no secondary phase formation which matches incredibly well with the JCPDS card no.74-2081 [11].On raising the pH there is a slight shift in the peak (311) and the peak value increases. This shift towards higher angle theta signifies the cation distribution in the lattice site. The crystallite size increases as the pH concentration in the solution increases (**Table 1**).The growth in the crystallite size is governed by the pH of the solution. The crystallite size was premeditated by Scherrer formula [12],

$$D = \frac{k\lambda}{\beta \cos\theta} \qquad (1)$$

$$\beta = (\beta_M^2 + \beta_S^2)^{\frac{1}{2}} \qquad (2)$$

Where 'λ' is 1.5406 Å for $CuK\alpha_1$, k is the instrumental constant, 'θ' is a Bragg's angle, β_M is the full width at half maximum of the peak (311), 'D' is the average particle size and $\beta_S$is the standard instrumental broadening. The lattice constant increases as the pH concentration increases there is a linear nature in the lattice constant which abides Vegard's law. The experimental lattice constant for $Ni_{0.5}Dy_{0.5}Fe_2O_4$ is calculated by the equation (3) [13],

$$a_{exp} = \frac{d}{\sqrt{h^2+k^2+l^2}} \qquad (3)$$

As the pH concentration increases the nickel ions are replaced by Dy^{3+} ions in the lattice site. On increasing the pH the peaks become narrow which intend shows the increase in crystallite size. The intensity of (311) peak decreases as the pH concentration increases, the growth of the particle depends on Oswald's ripening. [**Fig.1b**]. In $Ni_{0.5}Dy_{0.5}Fe_2O_4$ ionic radii of Dy^{3+} ion (1.03 Å), Ni^{2+} ion (0.69 Å) and Fe^{3+} ion (0.55 Å) [14]. Taking these features, cation distribution for the as-synthesized nanoparticles is depicted **Table 1**.

Table 1. Lattice parameter of $Ni_{0.5}Dy_{0.5}Fe_2O_4$ nanoparticles

pH	D (nm)	a_{exp} (nm)	a_{th} (nm)	U^{3m} (nm)	U (nm)
9	8.2	0.841	0.842	0.27066	0.3953
10	9	0.84	0.845	0.27051	0.3948
11	10.5	0.847	0.854	0.27046	0.3939
12	13	0.850	0.857	0.27039	0.3932

The mean ionic radius of tetrahedral (r_A) and octahedral sites ((r_B) is calculated by the below equation,

$$r_A = [C_{Dy2+}.r_{Dy2+} + C_{Ni2+}.r_{Ni2+} + C_{Fe3+}.r_{Fe3+}] \qquad (4)$$

$$r_B = (\tfrac{1}{2})[C_{Dy2+}.r_{Dy2+} + C_{Ni2+}.r_{Ni2+} + C_{Fe3+}.r_{Fe3+}] \qquad (5)$$

where, r is the ionic radii and c is the fractional concentration of cations in the sites. Mean radii of the tetrahedral site (B site) decreases as the pH concentration increases this is due to the Fe^{3+} ion in the octahedral site (B site). Theoretical calculation of the lattice parameter increases with increase of pH concentration is calculated by the equation (6),

$$a_{th} = \left(\frac{8}{3\sqrt{3}}\right)[(r_A + R_O) + 3(r_B + R_O)] \quad (6)$$

$$u = \left(\frac{1}{a_{th}\sqrt{3}}\right)(r_A + R_O) + 1/4 \quad (7)$$

$$U^{3m} = \frac{\frac{1}{4}R^2 - \frac{2}{3} + \left(\frac{11}{48}R^2 - \frac{1}{18}\right)}{2R^2 - 2} \quad (8)$$

The anion-cation length R_A and R_B are calculated using the following relation,

$$R_A = a\sqrt{3\left(\delta + \frac{1}{8}\right)} \quad (9)$$

$$R_B = a\left(\frac{1}{16} - \frac{\delta}{2} + 3\delta^2\right) \quad (10)$$

$$\delta = u - u_{ideal} \quad (11)$$

where, δ represents deviation ofoxygen positional parameter. The calculated values are tabulated in **Table 2**.

$$R = a(2)^{\frac{1}{2}}(2u - 0.5) \quad (12)$$

$$R' = a(2)^{\frac{1}{2}}(1 - 2u) \quad (13)$$

$$R'' = a(4u^2 - 3u + \frac{11}{16})^{\frac{1}{2}} \quad (14)$$

The bond angle calculated by cation-cation (p, q, r, s) cation-anion (b, c, d, e, f) are tabulated in **Table 3.** The magnetic interface is the contrariwise of the bond length [15], has been calculated by the below relation,

Cation –cation distance Cation –anion distance

$$b = \left(\frac{a}{4}\right)(2)^{1/2} \quad (15)$$

$$c = \left(\frac{a}{8}\right)(11)^{1/2} \quad (16)$$

$$d = \left(\frac{a}{4}\right)(3)^{1/2} \quad (17)$$

$$e = \left(\frac{3a}{8}\right)(3)^{1/2} \quad (18)$$

$$f = \left(\frac{a}{4}\right)(6)^{1/2} \quad (19)$$

$$p = a\left(\left(\frac{5}{8}\right) - u\right) \quad (20)$$

$$q = a\left(u - \frac{1}{4}\right)(3)^{1/2} \quad (21)$$

$$r = a\left(u - \frac{1}{4}\right)(11)^{1/2} \quad (22)$$

$$s = a\left(\left(\frac{1}{3u}\right) + \left(\frac{1}{8}\right)\right)(3)^{1/2} \quad (23)$$

Table 2 Interatomic sites of $Ni_{0.5}Dy_{0.5}Fe_2O_4$ nanoparticles

pH concentration	r_A	r_B	R_A	R_B	R	R'	R''	A-O	B-O
9	0.06570	0.0670	0.06584	0.0650	0.3230	0.2718	0.2980	0.19750	0.2009
10	0.06562	0.0683	0.06581	0.0657	0.3232	0.2724	0.2989	0.19757	0.2014
11	0.06550	0.0689	0.06564	0.0659	0.3235	0.2727	0.2993	0.19763	0.2017
12	0.06540	0.0694	0.06642	0.0660	0.3237	0.2733	0.2997	0.19767	0.2020

Table 3 Bond length between cations-cations and cation-anions

pH concentration	P	q	r	S	b	c	d	e	f
9	0.2010	0.1958	0.3655	0.3808	0.2931	0.3481	0.3615	0.5430	0.5143
10	0.2014	0.1961	0.3797	0.3761	0.2932	0.3493	0.3623	0.5448	0.5146
11	0.2019	0.1974	0.3810	0.3674	0.2937	0.3495	0.3635	0.5453	0.5148
12	0.2024	0.1983	0.3817	0.3670	0.2943	0.3580	0.3639	0.5461	0.5151

Table.4 FTIR bands of $Ni_{0.5}Dy_{0.5}Fe_2O_4$ nanoparticles

pH concentration	$\nu_1 \times 10^{-2}$ m^{-1}	$\nu_2 \times 10^{-2}$ m^{-1}	k_t X 10^{-2} (1/m)	k_0 X 10^{-2} (1/m)	C_{11} GPa	C_{12} GPa
9	564	460	90.365	40.230	78.104	36.541
10	553	456	90.370	41.563	78.489	36.978
11	550	443	90.376	43.432	79.634	37.537
12	539	418	90.382	43.724	91.813	40.678

3.2 FTIR analysis

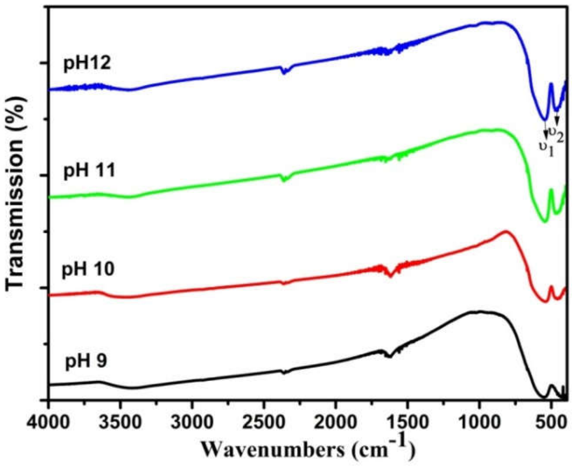

Fig.3 FTIR spectrum of $Ni_{0.5}Dy_{0.5}Fe_2O_4$ nanoparticles

The FTIR spectra of $Ni_{0.5}Dy_{0.5}Fe_2O_4$ nanoparticles consist of two broad vibrational bands in the range of 400-600 cm^{-1}. These bands are assigned to the stretching vibrational modes of metal ions in tetrahedral site ν_1 (M_A-O) and octahedral site ν_2 (M_B-O). In mixed ferrites on substituting rare earth shows a strong negotiation in the vibrational band, as the pH concentration there is a steady variation in cations sites this ensures the inverse spinel formation remains unaltered [16]. This distribution in the cation site strongly effects the vibration of lattice. On increasing pH concentration, the spectra show a significant shift in peak to higher frequency range, this is payable to the trepidation happening in Fe^{3+} ions site. Usually, the bond length of ferrite ions in octahedral site is lower than the tetrahedral site, which is due to the covalent bonding of Fe^{3+} ions. The force constants (k_o) and the absorption band position (k_t) and k_o is calculated by using the equation (24, 25),

$$k_t = 7.62\ M_A \nu_1^2 \times 10^{-7} N/m \qquad (24)$$

$$k_o = 5.31\ M_B \nu_2^2 \times 10^{-7} N/m \qquad (25)$$

where, M_A is the molecular weight of A – site and M_B is the molecular weight of B – sites cations. The stiffness constant (C_{11}&C_{12}) are calculated by the below relation,

$$C_{11} = k_{av} / a_c \qquad (26)$$

$$C_{12} = (\sigma C_{11}) / (1 - \sigma) \qquad (27)$$

The relations of stiffness constant of the $Ni_{0.5}Dy_{0.5}Fe_2O_4$ nanoparticles is calculated and presented in **Table.4.**

3.2 UV-visible analysis

A UV-visible spectrum is used to determine the optical properties of as-synthesized samples. The gap edged by absorbance is due to the incidence of electron-photon interactions, interface defects and point defects [17]. The red shift emerges owing to the metastable states within the band edge. The indirect band gap was estimated by the extrapolation of the x-axis in the graph by Tauc's plot as shown in **Fig. 4**. The absorption edge is calculated by using the relation,

$$\alpha h v = A(hv - Eg)^{1/2} \qquad (28)$$

where, h, υ, and A are the Planck constant, absorption coefficient and light frequency and Eg is the band gap, α is the proportionality constant.

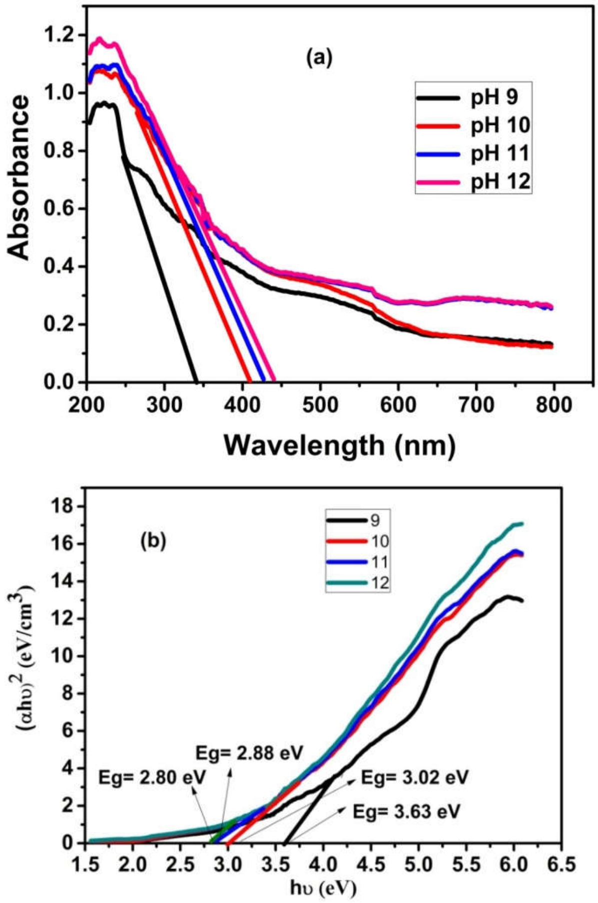

Fig.4 (a) and (b) UV-vis spectrum and bandgap energy plot of $Ni_{0.5}Dy_{0.5}Fe_2O_4$ nanoparticles

The band gap decreases as the pH concentration increases which is due to the quantum confinement. The band gap is influenced by various factors like annealing temperature, particle size, lattice parameters, presence of secondary phase and impurities. the absorption edge of ferrite nanoparticles in the visible region is due to the excitation of electrons from O2p state to Fe3d state which is rational for the inverse spinel nanoparticles [18].

3.2.1 Photocatalytic activity

Photo-Fenton activity of $Ni_{0.5}Dy_{0.5}Fe_2O_4$ nanocrystals was observed by the dilapidation of property in organic dye which was irradiated to visible light with a 125 W mercury as a irradiation light source. In this experiment 50 mg of photo-catalyst was dispersed in 50 ml of 10 mg/l of MB solution. Prior to irradiating, the solution was stirred in the absence of light for 30 minutes to make definite desorption-adsorption equilibrium of MB aqueous solution with the nanocatalyst ($Ni_{0.5}Dy_{0.5}Fe_2O_4$).

Then the aqueous solution with the catalyst was exposed to light after addition of 2 ml of 30% H_2O_2. At given time intervals, 3 ml of aliquots were centrifuged in order to remove ferrite nanoparticles. The concentration of MB was observed with the UV-vis spectrophotometer is observed in Fig.5. The percentage of degradation of Methylene blue is listed in the table. 5, the efficiency of degradation depends on the particle size shown in Fig.6.

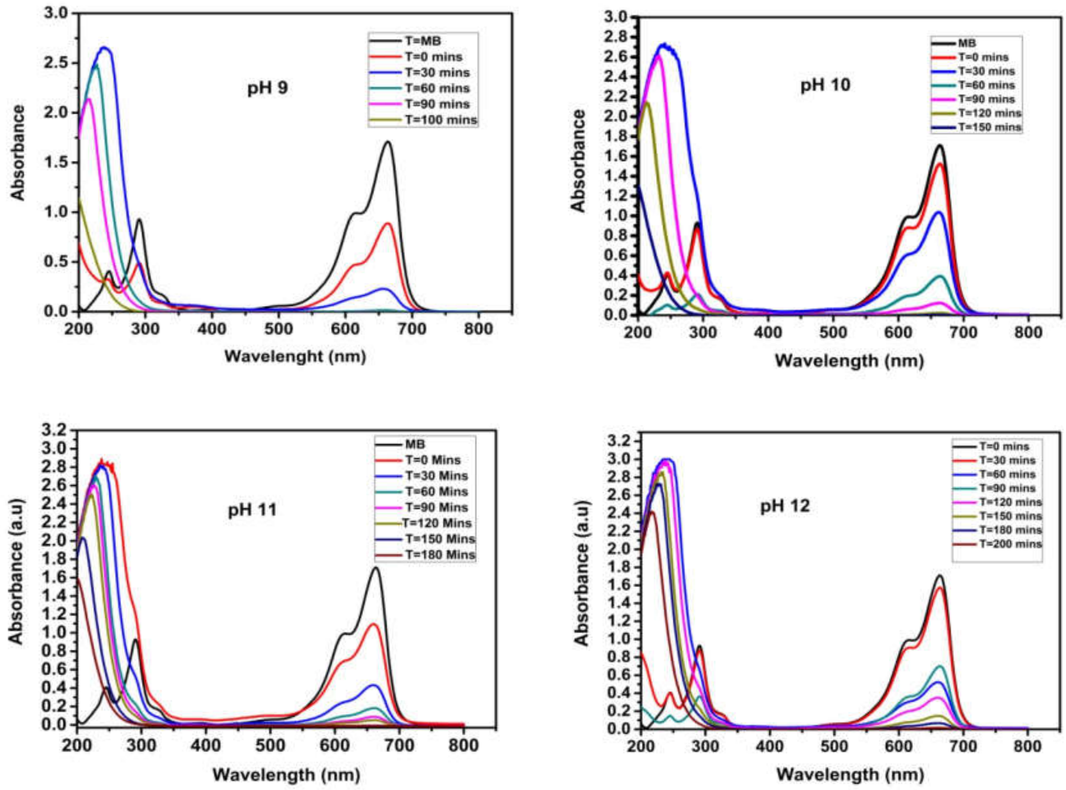

Fig.5 Degradation spectra of MB with respect to time in the presence of $Ni_{0.5}Dy_{0.5}Fe_2O_4$ nanocatalyst

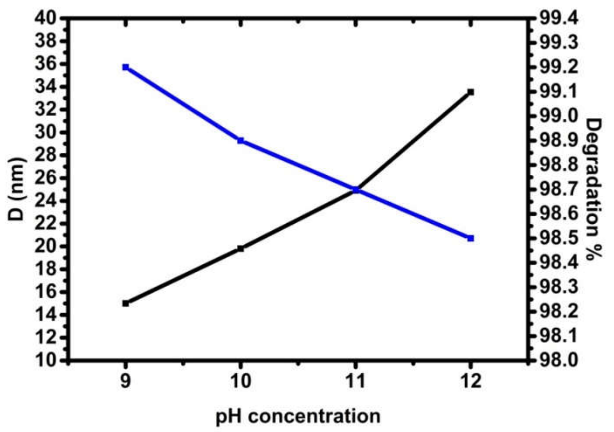

Fig.6 Dependence of crystallite size with degradation%

3.2. 2Chemical kinetics

The degradation of organic MB in the presence of catalyst follows pseudo first order kinetics and the rate constant is calculated using Langmuir-Hinshelwood model [19], Fig.7 shows the linear relation between irradiation andln $\left(\frac{C}{Co}\right)$.

$$kt = \ln\left(\frac{C}{Co}\right) \qquad (29)$$

Table.5 Degradation of crystallite size and degradation rate constant

pH	D (nm)	Degradation (%)	Rate constant
9	15.01	99.2	0.006
10	19.81	98.9	0.008
11	24.91	98.7	0.012
12	35.53	98.5	0.021

3.2.3 Recyclability

Recyclability of the $Ni_{0.5}Dy_{0.5}Fe_2O_4$ catalyst is of primary connotation for industrial waste water treatment in long term progression to mortify the organic pollutants present in the water. Ferrites own first-rate photo-Fenton activity, hence can be easily separated using magnetic fields. After degradation of MB, the nanocatalyst was centrifuged with distilled water, followed by drying at 75 °C for 24 hours in a hot air oven. The ferrite nanoparticles had no crucial trouncing even after five cycles hence confirm their importance in treating waste water from industries. The typical degradation percentage of organic dye in the presence of $Ni_{0.5}Dy_{0.5}Fe_2O_4$ nanoparticles for 5 successive cycles is shown in Fig.8.

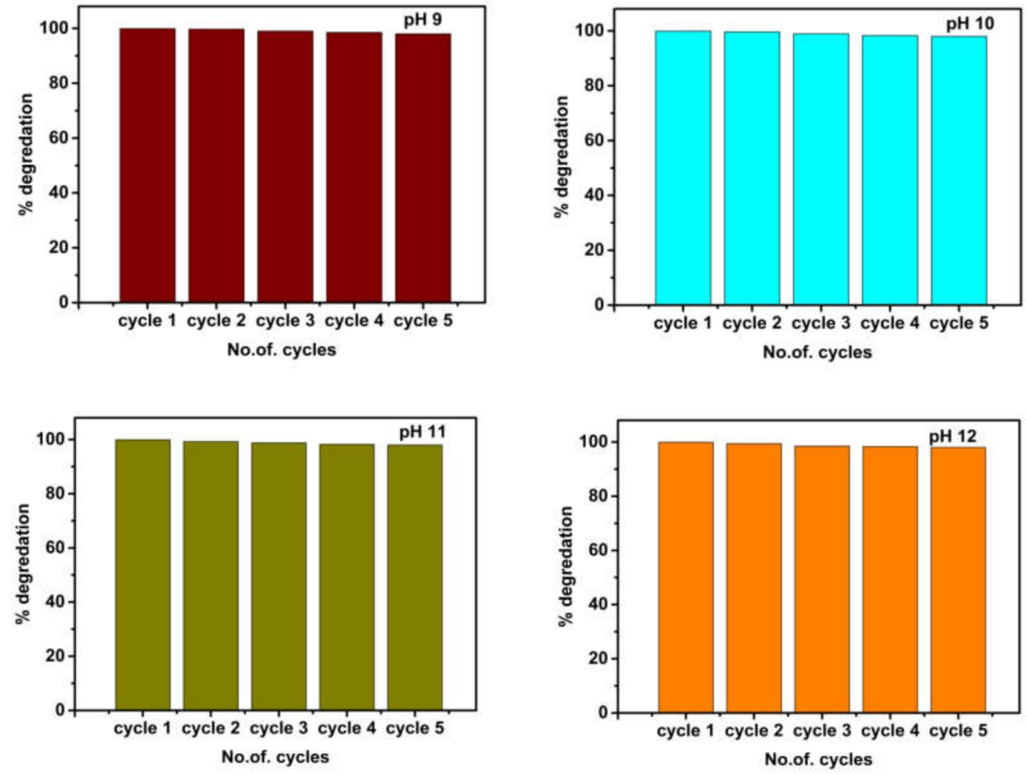

Fig.7 Degradation kinetics of $Ni_{0.5}Dy_{0.5}Fe_2O_4$ nanoparticles

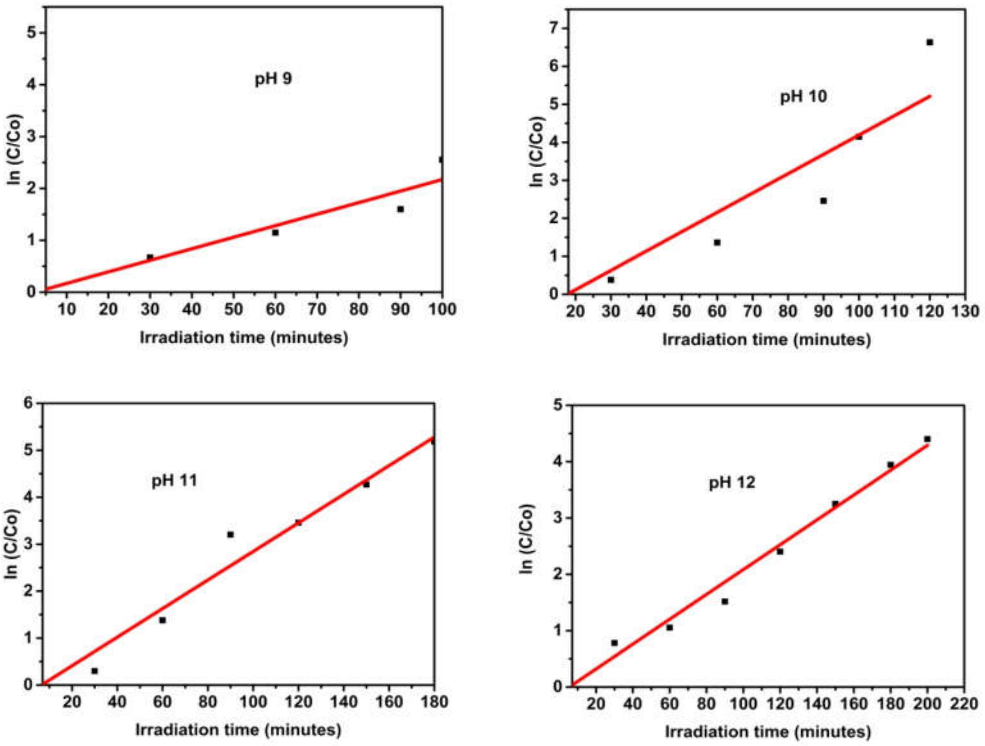

Fig. 8 Recyclability of $Ni_{0.5}Dy_{0.5}Fe_2O_4$ for 5 consecutive cycles

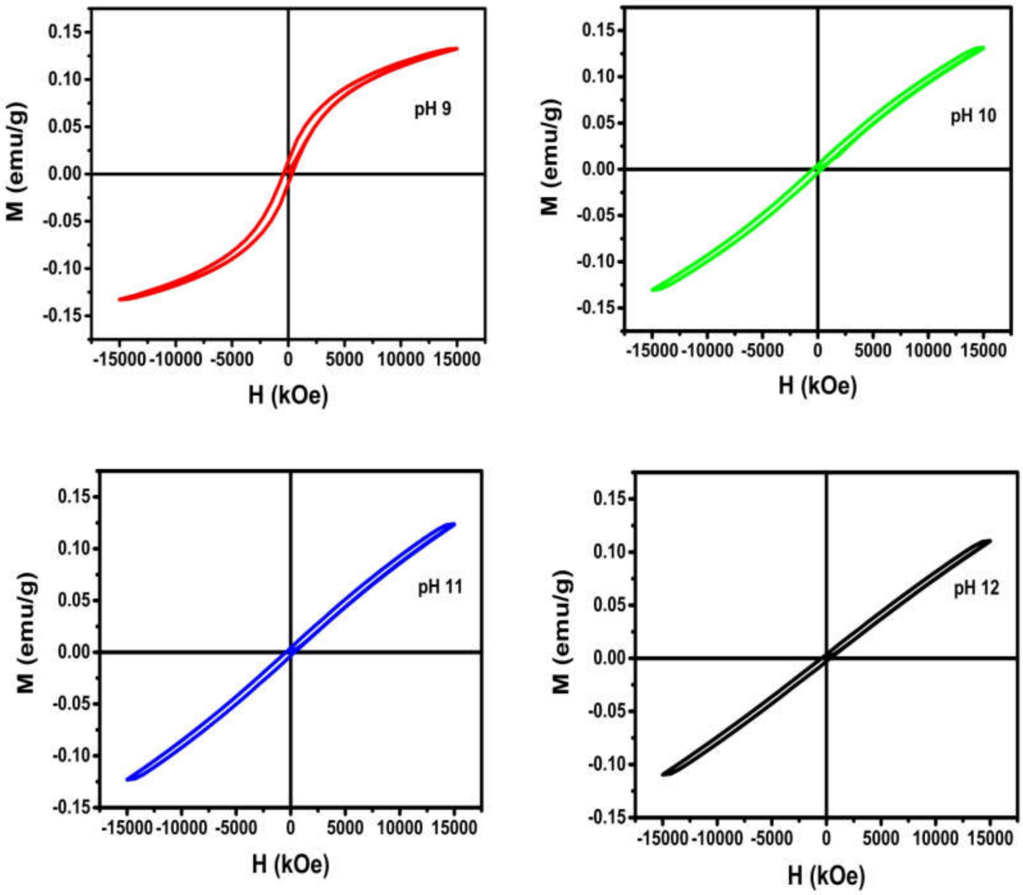

Fig.9 VSM of $Ni_{0.5}Dy_{0.5}Fe_2O_4$ nanoparticles

3.3 VSM analysis

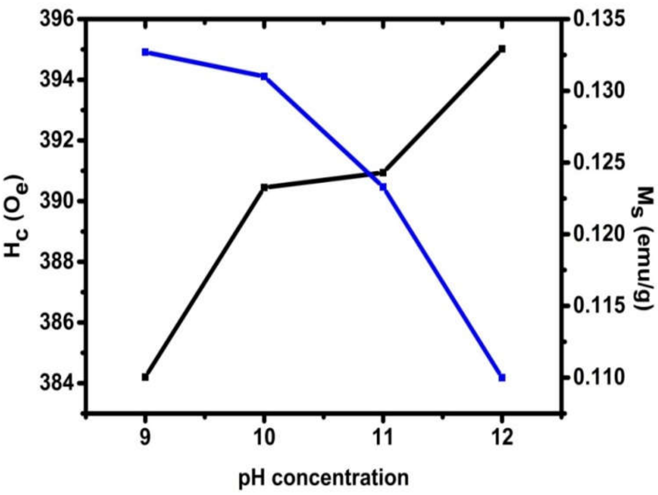

Fig.10 Dependence of coercivity and saturation magnetization with pH variation

The magnetic measurements for the as-synthesized sample analyzed by the vibrating sample magnetometer at room temperature with an applied field of 10KOe are depicted in Fig.9. The magnetic property depends on the quantum coupling like S-S coupling and L-S coupling, here the nanoparticles possess a magnetic domain due to the cation distribution. The saturation magnetization decreases drastically as the coercivity decreases which is due to the magnetization changes in the domain wall and also due to the surface effects in the finite size scaling in nano surface. The quantum mechanical potential model and O-2p electron model plays an important role in cation distribution that leads to the magnetic moment in the cation site [20].

The magnetic moment (μ_B) for the as-synthesized nanocrystal is calculatedby the relation,

$$\mu_B = \frac{M \times M_s}{5855} \quad (30)$$

where, M is the molar mass, M_s is the saturation magnetization and μ_B is the magnetic moment. In $Ni_{0.5}Dy_{0.5}Fe_2O_4$ nanoparticles, Dy^{3+}ions occupy the tetrahedral site while Fe^{2+}ions preferoctahedral site. This cation distribution is sturdily reliant on the synthesis technique. The retentivity (M_r), coercivity (H_c), saturation magnetization (M_s) and magnetic moment (μ_B) for the synthesized samples are given in table 6. The hysteresis loop specifies definite ordering of spin states and the nanosamples possesses a ferromagnetic nature. It was evident that as the pH, concentration increases, the corecivity increases whereas saturation magnetization decreases as shown in Fig.10.

Table.6 Corecivity (H_c), Squareness ratio (M_r/M_s), Retentivity (M_r), Saturation Magnetization (M_s) and Magnetic moment (μ_B) of $Ni_{0.5}Dy_{0.5}Fe_2O_4$nanoparticles.

pH	$H_c(O_e)$	M_s(emu/g)	M_r(emu/g)	μ_B
9	395.02	0.13270	11.929	0.00546
10	390.94	0.13104	4.237	0.00539
11	370.21	0.12339	3.7031	0.00508
12	354.20	0.11009	3.1544	0.00453

4 Conclusions

The prime emphasis of the current work is to synthesize highly crystalline nanocrystals, which had its significant effect on magnetic properties. From FTIR spectrum, the functional group was determined with the stretching vibrations present in octahedral and tetrahedral site. The UV-vis spectrum reveals the optical property of the as-synthesized nanocrystals. A VSM measurement discloses the ferromagnetic nature of the crystal with respect to the domain wall is studied. The $Ni_{0.5}Dy_{0.5}Fe_2O_4$nanocrystals is considered to have astonishing and impending significance in photo-Fenton activity.

References

[1] Rodney, John D., S. Deepapriya, P. Annie Vinosha, S. Krishnan, S. Janet Priscilla, R. Daniel, and S. Jerome Das. "Photo-Fenton degradation of nano-structured La doped CuO nanoparticles synthesized by combustion technique." Optik 161 (2018): 204-216.

[2] Sharma, Rimi, and Sonal Singhal. "Structural, magnetic and electrical properties of zinc doped nickel ferrite and their application in photo catalytic degradation of methylene blue." Physica B: Condensed Matter 414 (2013): 83-90.

[3] Rath, Chandana, S. Anand, R. P. Das, K. K. Sahu, S. D. Kulkarni, S. K. Date, and N. C. Mishra. "Dependence on cation distribution of particle size, lattice parameter, and magnetic properties in nanosize Mn–Zn ferrite." Journal of Applied Physics 91, no. 4 (2002): 2211-2215.

[4] Sharma, Rohit, Prashant Thakur, Manoj Kumar, Pankaj Sharma, and Vineet Sharma. "Nanomaterials for high frequency device and photocatalytic applications: Mg-Zn-Ni ferrites." Journal of Alloys and Compounds 746 (2018): 532-539.

[5] Sharma, Rohit, Prashant Thakur, Manoj Kumar, Pankaj Sharma, and Vineet Sharma. "Nanomaterials for high frequency device and photocatalytic applications: Mg-Zn-Ni ferrites." Journal of Alloys and Compounds 746 (2018): 532-539.

[6] Maaz, K., S. Karim, A. Mumtaz, S. K. Hasanain, J. Liu, and J. L. Duan. "Synthesis and magnetic characterization of nickel ferrite nanoparticles prepared by co-precipitation route." Journal of Magnetism and Magnetic Materials 321, no. 12 (2009): 1838-1842.

[7] Sagadevan, Suresh, Zaira Zaman Chowdhury, and Rahman F. Rafique. "Preparation and Characterization of Nickel ferrite Nanoparticles via Co-precipitation Method." Materials Research AHEAD (2018)

[8] Shen, Wei, Leihao Zhang, Bowen Zhao, Yichun Du, and Xing Zhou. "Growth mechanism of octahedral like nickel ferrite crystals prepared by modified hydrothermal method and morphology dependent magnetic performance." Ceramics International (2018).

[9] Bhasker, S. Uday, G. Narsinga Rao, F. C. Chou, and MV Ramana Reddy. "Temperature dependent and applied field strength dependent magnetic study of Cobalt Nickel ferrite nano particles: Synthesized by an environmentally benign method." Journal of Magnetism and Magnetic Materials (2018).

[10] Kokare, M. K., Nitin A. Jadhav, Yogesh Kumar, K. M. Jadhav, and S. M. Rathod. "Effect of Nd 3+ doping on structural and magnetic properties of Ni 0.5 Co 0.5 Fe 2 O 4 nanocrystalline ferrites synthesized by sol-gel auto combustion method." Journal of Alloys and Compounds (2018).

[11] Anjana, V., Sara John, Pooja Prakash, Amritha M. Nair, Aravind R. Nair, SreedhaSambhudevan, and Balakrishnan Shankar. "Magnetic Properties of Copper Doped Nickel Ferrite Nanoparticles Synthesized by Co Precipitation Method." In IOP Conference Series: Materials Science and Engineering, vol. 310, no. 1, p. 012024. IOP Publishing, 2018.

[12] Rao, B. Parvatheeswara, B. Dhanalakshmi, S. Ramesh, and PSV Subba Rao. "Cation distribution of Ni-Zn-Mn ferrite nanoparticles." Journal of Magnetism and Magnetic Materials456 (2018): 444-450.

[13] Babu, K. Vijaya, G. Satyanarayana, B. Sailaja, GV Santosh Kumar, K. Jalaiah, and M. Ravi. "Structural and magnetic properties of Ni0. 8M0. 2Fe2O4 (M= Cu, Co) nano-crystalline ferrites." Results in Physics 9 (2018): 55-62.

[14] Rao, B. Parvatheeswara, B. Dhanalakshmi, S. Ramesh, and PSV Subba Rao. "Cation distribution of Ni-Zn-Mn ferrite nanoparticles." Journal of Magnetism and Magnetic Materials456 (2018): 444-450.

[15] Sendhilnathan, S. "Enhancement in dielectric and magnetic properties of Mg2+ substituted highly porous super paramagnetic nickel ferrite nanoparticles with Williamson-Hall plots mechanistic view." Ceramics International 43, no. 17 (2017): 15447-15453.

[16] Khan, Ayaz Arif, M. Javed, A. Rauf Khan, Yousaf Iqbal, Asif Majeed, Syed Zahid Hussain, and S. K. Durrani. "Influence of preparation method on structural, optical and magnetic properties of nickel ferrite nanoparticles." Materials Science-Poland 35, no. 1 (2017): 58-65.

[17] Fardood, SaeidTaghavi, KobraAtrak, and Ali Ramazani. "Green synthesis using tragacanth gum and characterization of Ni–Cu–Zn ferrite nanoparticles as a magnetically separable photocatalyst for organic dyes degradation from aqueous solution under visible light." Journal of Materials Science: Materials in Electronics 28, no. 14 (2017): 10739-10746.

[18] De, Manojit, SoumenBera, and Hari ShankerTewari. "Structural characterization of magnesium-substituted nickel ferrite nanoparticles" Emerging Materials Research 6, no. 2 (2017): 265-269.

[19] Anjana, V., Sara John, Pooja Prakash, Amritha M. Nair, Aravind R. Nair, SreedhaSambhudevan, and Balakrishnan Shankar. "Magnetic Properties of Copper Doped Nickel Ferrite Nanoparticles Synthesized by Co Precipitation Method." In IOP Conference Series: Materials Science and Engineering, vol. 310, no. 1, p. 012024. IOP Publishing, 2018.

[20] Saranya, R., R. Azhagu Raj, M. S. AlSalhi, and S. Devanesan. "Dependence of Catalytic Activity of Nanocrystalline Nickel Ferrite on Its Structural, Morphological, Optical, and Magnetic Properties in Aerobic Oxidation of Benzyl Alcohol." Journal of Superconductivity and Novel Magnetism 31, no. 4 (2018): 1219-1225